

Direct Superpoints Matching for Fast and Robust Point Cloud Registration

Aniket Gupta Yiming Xie Hanumant Singh Huaizu Jiang
Northeastern University
{gupta.anik, xie.yim, ha.singh, h.jiang}@northeastern.edu

Abstract

Although deep neural networks endow the downsampled superpoints with discriminative feature representations, directly matching them is usually not used alone in state-of-the-art methods, mainly for two reasons. First, the correspondences are inevitably noisy, so RANSAC-like refinement is usually adopted. Such ad hoc postprocessing, however, is slow and not differentiable, which can not be jointly optimized with feature learning. Second, superpoints are sparse and thus more RANSAC iterations are needed. Existing approaches use the coarse-to-fine strategy to propagate the superpoints correspondences to the point level, which are not discriminative enough and further necessitates the postprocessing refinement. In this paper, we present a *simple yet effective* approach to extract correspondences by *directly matching* superpoints using a global softmax layer in an end-to-end manner, which are used to determine the rigid transformation between the source and target point cloud. Compared with methods that directly predict corresponding points, by leveraging the rich information from the superpoints matchings, we can obtain more accurate estimation of the transformation and effectively filter out outliers *without any postprocessing refinement*. As a result, our approach is not only fast, but also achieves state-of-the-art results on the challenging ModelNet and 3DMatch benchmarks. Our code and model weights will be publicly released.

1 Introduction

Point cloud registration refers to the task of aligning two partially overlapping point clouds into a shared coordinate system. In this paper, we tackle the problem of rigid registration where the goal is to determine the optimal transformation matrix, including rotation and translation, from one point cloud (source) to the other (target). It has attracted a lot of research interest due to its broad applications in SLAM (Simultaneous Localization and Mapping) [16, 50], autonomous driving [34, 37], 3D reconstruction [26, 22], etc.

A prevailing paradigm to solve the registration task is to leverage the correspondences of *superpoints* across two point clouds, which can be obtained either using separate keypoint detectors [1, 4, 13, 24] to capture salient and distinctive points or regions within a point cloud. With the rapid advancement in representation learning in point clouds using deep neural networks [42, 43, 51], the keypoint-free approaches have gained significant attention, where the point cloud is downsampled into superpoints. Although they may not be designed to capture the salient keypoints in the point cloud, the learned representations endow the superpoints with discriminative power so they can be matched across the source and target point clouds. The transformation matrix can then be obtained based on the superpoints correspondences using the Kabsh-Umeyama Algorithm [53, 28].

Direct superpoint matching is typically not used by itself in existing approaches for point cloud registration for two reasons. First, the correspondences of superpoints inevitably contain errors, either because the point clouds contain noisy sensory data or because some of the correspondences are simply

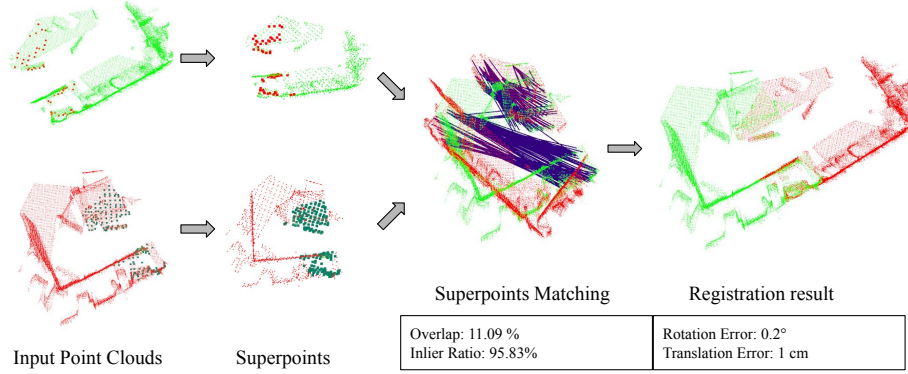


Figure 1: Our approach focuses on directly matching the predicted superpoints by computing correlation between them. The bold dots show the superpoints with highest correlation which are used as correspondences to correctly register the point cloud pair.

incorrect. As a result, postprocessing refinement is usually needed, for instance, using RANSAC to prune out the outliers [13, 14, 68]. However, RANSAC is inherently slow and not differentiable, and thus cannot be integrated into the training step. Second, superpoints are essentially sparse, particularly because of downsampling in neural networks. Therefore, more RANSAC iterations are needed as the number of inliers (*i.e.*, correct correspondences) is small, which imposes a significant computation burden. To this end, the *coarse-to-fine* registration scheme is usually adopted in state-of-the-art approaches [44, 66, 38], where superpoints correspondences serve as coarse correspondences only. They are then propagated to the point level, forming finer-level correspondences. Since point-wise features only capture local information, they lack enough discriminative power. Consequently, the noise in the point-wise correspondences is more prominent, which further necessitates the additional refinement step. Although the Local to Global Registration (LGR) module introduced in [44] improves the speed, which works similarly to RANSAC in an iterative manner, the selection and refinement of the transformation still remain non-differentiable. The entire model thus can not be optimized jointly, leading to inferior accuracy.

In this paper, we present a *simple yet effective* approach for rigid point cloud registration by *directly matching the superpoints*. Specifically, superpoints features are first obtained from the KPConv backbone [51], which are then enhanced using Transformer blocks with interleaved multi-head self and cross attention modules [64], enabling effective learning of the structural information of from the target to the source point cloud. The enhanced superpoint features are finally matched using a Global Softmax layer inspired by the 2D matching work [60], which generates a correlation matrix capturing the pairwise relationships between the keypoints from the source and target point clouds. But unlike [60], we fully harness the rich information in the correlation matrix. We employ a differentiable variant of the Kabsh-Umeyama Algorithm [53, 28], considering the strengths of matchings, where the weights of the SVD (Singular Value Decomposition) are the correlation scores between two corresponding superpoints. By examining the correlation scores of the superpoints, we can easily identify the highly reliable correspondences without resorting to the time-consuming RANSAC or the non-differentiable LGR module [44]. Our approach is fully differentiable and can be trained in an end-to-end manner, which enables joint optimization of the feature representation learning, superpoints matching, and transformation estimation, leading to improved alignment results. Moreover, our approach does not require ad-hoc postprocessing, *e.g.*, RANSAC, it runs fast, making it potentially more useful in practice. Compared with the recent end-to-end method [64], our approach directly matches the superpoints. With the rich information obtained from the matching step, our approach can get a more accurate estimation of the transformation between the point clouds robustly by filtering out the outliers effectively.

We run experiments on standard benchmarks, including ModelNet [58] and 3DMatch [68], and achieve state-of-the-art results. Extensive ablation studies validate the effectiveness of each module in our proposed approach. The key contributions of the paper can be summarized as follows:

- **Efficiency.** Our approach tackles the point cloud registration by directly matching superpoints. The rich information in the matching step allows us to effectively filter out outliers without using RANSAC-like approaches. As a result, our approach is efficient and runs fast in practice.
- **Simplicity.** Our registration pipeline can be trained end-to-end without the any ad hoc postprocessing refinement. It streamlines the process and makes it more straightforward to implement and understand.
- **Robustness.** We thoroughly evaluate our method on various datasets, demonstrating its superior performance in comparison to existing techniques. Our approach achieves state-of-the-art results on multiple benchmarks, with notably high inlier ratios. This showcases the robustness and accuracy of our proposed registration framework.

2 Related Work

Traditional registration approaches. The most known algorithm Iterative Closest Point (ICP) [5] has been widely used for point cloud registration. ICP solves the registration problem iteratively in two steps: (1) It obtains the spatially closest point correspondence and then (2) finds the least-squares rigid transformation. The spatial-distance-based correspondences are sensitive to the initial transformation and point noises. A lot of variants [46, 11, 49, 6, 45, 35] have been proposed to improve ICP. Another line of work [27, 17] formulates the point cloud registration as probability distribution matching problems to improve the robustness and to converge quickly. However, they still heavily rely on an appropriate initialization and can easily converge to a local optimum as opposed to the global solution. Unlike the local methods mentioned above, global approaches are invariant to the initialization. Based on branch-and-bound techniques, several works [61, 8, 9, 35] have been proposed, but they are very slow and impractical in some scenarios. Another method is to extract and match keypoints based on feature extraction methods such as FPFH [47] and SHOT [52]. Then RANSAC [18] can be used for registration. However, RANSAC is computationally very slow compared to ICP.

Learning-based registration approaches. Recently, many works have used deep learning for point cloud learning and registration. Some work first estimates the correspondence between two point clouds and then computes the transformation with some robust pose estimators. To predict the correspondence between two point clouds, 3DMatch [68] detects the repeatable keypoints and learns discriminative descriptors for keypoints. The following works aim to either improve the keypoint detections [4, 32, 62] or learn better feature descriptors [13, 14, 15, 29, 1, 55]. Predator [24] uses the attention mechanism proposed in Transformers [54] to enhance the point feature descriptors. Other detector-free methods [66, 44] extract the correspondences by considering all possible matches. Another line of work [10, 67] has included the transformation computation into the training pipeline. Following the idea of ICP [5], [57, 56, 63, 19, 31] iteratively predict the soft correspondences and computes the transformation with differentiable weighted SVD. Another way [2, 33, 25, 59, 48] first extracts a global feature vector for each point cloud and predicts the transformation with global feature vectors. This approach usually fails in large-scale scenes. Unlike these works which require either ad-hoc postprocessing or coarse-to-fine registration, our method directly matches the superpoints without any refinement.

Correspondence filters. RANSAC [18] is typically used to filter out the outliers in the predicted correspondence to obtain a robust transformation estimation. However, RANSAC is relatively slow and cannot be incorporated into the training pipeline because the hypothesis selection step is non-differentiable. To alleviate these problems, DSAC [7] modify the RANSAC pipeline and make it differentiable. Other deep robust estimators [3, 12, 40, 20, 30, 65] usually use the classification network to identify which correspondences are outliers and then reject them. Instead of using these complex correspondence filters, our method can directly filter out outliers effectively by leveraging the rich information in the superpoints matching.

3 Method

Given the source and target point clouds $\mathbf{X} \in \mathbb{R}^{M \times 3}$ and $\mathbf{Y} \in \mathbb{R}^{N \times 3}$, our goal is to determine the optimal rigid transformation $\mathbf{T} = \{\mathbf{R}, \mathbf{t}\}$ with rotation $\mathbf{R} \in SO(3)$ and translation $\mathbf{t} \in \mathbb{R}^3$ to align two point clouds into a common coordinate system. M and N denote the numbers points.

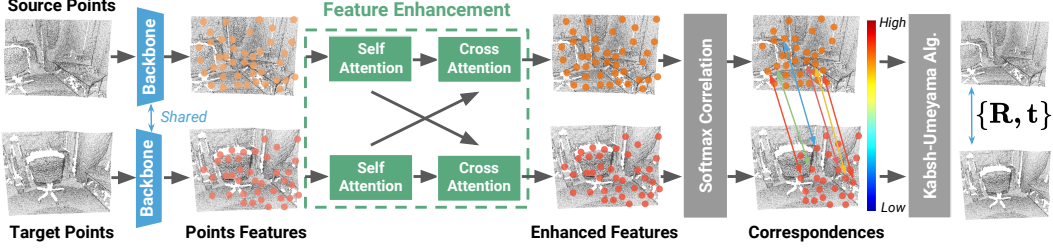


Figure 2: **Model Architecture:** The KPConv backbone downsamples the input point cloud and generates superpoints and superpoint feature vectors. These superpoint features are then conditioned on the other point cloud in the Feature Enhancement block. Lastly, superpoint features can be directly matched using Global Softmax to predict correspondences and estimate rigid transformation.

3.1 Superpoints Feature Extraction and Enhancement

In our approach, we use Kernel Point Convolution (KPConv) [51] as the backbone to selectively downsample the point cloud into a set of superpoints and extract global feature vectors for each superpoint. Specifically, the KPConv backbone uses a series of ResNet-like blocks [23] and convolutions to downsample the input point clouds into a reduced set of superpoints $\mathbf{X}' \in \mathbb{R}^{M' \times 3}$ and $\mathbf{Y}' \in \mathbb{R}^{N' \times 3}$, where $M' < M$ and $N' < N$. The superpoints are described by their feature vectors $\mathbf{F}_{\mathbf{X}'} \in \mathbb{R}^{M' \times D}$ and $\mathbf{F}_{\mathbf{Y}'} \in \mathbb{R}^{N' \times D}$, respectively, with D being the feature dimension. The network weights are shared among the two point clouds. We use a shallower backbone for 3DMatch dataset compared to [64, 24] to avoid significant downsampling.

Although KPConv backbone provides reasonably good representations, the superpoints features are obtained within each point cloud *independently*. To obtain highly discriminative feature representations for superpoints matching, we further enhance their feature representations in the source point cloud to be conditioned on the target one and vice-versa. Following the previous work of point cloud registration [64] and the 2D counterpart of superpoints matching (*e.g.*, optical flow) [60], we adopt the multi-head attention mechanism in the Transformer model [54] as the feature enhancement module, shown in Fig. 2. It consists of both self and cross-attention, where the self-attention is to integrate the information from the other points within the same point cloud and the cross-attention allows interactions with points in another point cloud to consider the mutual dependencies. In addition to the multi-head attention, other components in the Transformer model, including position encodings of 3D points, residual connections, layer normalization, and feed-forward network are applied to each layer. The entire feature enhancement module consists of 6 such layers with 256 dimensions and 8 attention heads.

The outputs of the feature enhancement module are features $\bar{\mathbf{F}}_{\mathbf{X}'} \in \mathbb{R}^{M' \times D}$ and $\bar{\mathbf{F}}_{\mathbf{Y}'} \in \mathbb{R}^{N' \times D}$ which has aggregated geometric information from both source and target point cloud. The strongly associated features are strengthened while the weakly associated features are weakened. With such highly discriminative feature representations, we can obtain high-quality superpoints matchings.

3.2 Direct Superpoint Matching for Rigid Transformation Estimation

To get the correspondences between two point clouds, we first compare the feature similarity for each point in $\bar{\mathbf{F}}_{\mathbf{X}'}$ to all points in $\bar{\mathbf{F}}_{\mathbf{Y}'}$ by computing their correlations [60], which can be done efficiently in a single step as follows:

$$\mathbf{C} = \text{softmax}(\bar{\mathbf{F}}_{\mathbf{X}'} \bar{\mathbf{F}}_{\mathbf{Y}'}^T) \in \mathbb{R}^{M' \times N'}, \quad (1)$$

where \mathbf{C} is the normalized correlation matrix that represents the similarity between two point clouds. Based on the correlation matrix, the correspondences $\hat{\mathbf{Y}}$ and $\hat{\mathbf{X}}$ can be directly calculated by using the largest correlation for each point.

The rigid transformation between the source and target point clouds can be then estimated using the superpoints correspondences with a weighted variant of the Kabsch-Umeyama algorithm [28, 53]:

$$\hat{\mathbf{R}}, \hat{\mathbf{t}} = \arg \min_{\mathbf{R}, \mathbf{t}} \sum_i^{\min(N', M')} w_i \|\mathbf{R} \hat{\mathbf{x}}_i + \mathbf{t} - \hat{\mathbf{y}}_i\|^2, \quad (2)$$

where $\hat{\mathbf{x}}_i, \hat{\mathbf{y}}_i$ are two matched superpoints, denoting the i^{th} point in $\hat{\mathbf{X}}, \hat{\mathbf{Y}}$, respectively. The coefficient w_i can be used to weigh different correspondences.

Although we use the highly discriminative feature representations enhanced by the attention module, the correspondences are inevitably noisy. How to filter out the outliers (*i.e.*, incorrect correspondences)? We show that the normalized correlation matrix \mathbf{C} obtained from superpoints matching in Eq. (1) contains *rich information*, which allows us effectively select high-confident superpoints correspondences to estimate the transformation. Specifically, if $\hat{\mathbf{x}}_i$ is similar to multiple superpoints, *e.g.*, because of the repetitive patterns, its matching to $\hat{\mathbf{y}}_i$ tends to be unreliable. Therefore, the normalized correlation score between them will be low since \mathbf{C} is normalized w.r.t. all other superpoints in the target point cloud. We can therefore set $w_i = \mathbf{C}(\hat{\mathbf{x}}_i, \hat{\mathbf{y}}_i)$, capturing the confidence of the superpoints matchings. On the other hand, we can use w_i to select only highly confident superpoint matchings, *e.g.*, top 15% of them, to estimate the transformation in Eq.(2). We can also augment the weights w_i by considering the overlap score, which is introduced below, to further improve the accuracy.

Compared to previous work [44, 66, 38], our approach is *simple yet effective*, which does not only eliminates the coarse-to-fine strategy but more importantly, the slow and non-differentiable RANSAC. As a result, our approach is fast and the superpoints feature learning, superpoints matching, and transformation estimation can be optimized jointly in an end-to-end manner, leading to superior accuracy. Although the feature enhancement module is also used in [64], our approach is fundamentally different. Instead of predicting the correspondences by using the feature representations of the source point cloud only, we perform superpoints matching and use the rich information in the matching step to effectively filter outliers and get a robust estimation of the transformation.

3.3 Loss Functions

We train our approach using the following three loss functions, where the transformation loss is the main loss term and the other two are auxiliary ones.

Transformation Loss. We apply a L1 loss on the predicted transformed locations of all keypoints with the predicted and ground truth transformation matrix.

$$\mathcal{L}_T = \frac{1}{M'} \sum_i^{M'} \left| \hat{\mathbf{R}}\mathbf{x}'_i + \hat{\mathbf{t}} - (\mathbf{R}_{gt}\mathbf{x}'_i + \mathbf{t}_{gt}) \right|_1. \quad (3)$$

Overlap Loss. Inspired by [64], we estimate the overlap values $\hat{\mathbf{O}}_{\mathbf{X}'}$ and $\hat{\mathbf{O}}_{\mathbf{Y}'}$ using a separate MLP layer based on the enhanced feature $\bar{\mathbf{F}}_{\mathbf{X}'}$ and $\bar{\mathbf{F}}_{\mathbf{Y}'}$, respectively. The overlap estimation is formulated as a binary classification problem, so we use binary cross-entropy loss:

$$\mathcal{L}_o^X = -\frac{1}{M'} \sum_i^{M'} o_{x,i}^* \cdot \log \hat{o}_{x,i}^* + (1 - o_{x,i}^*) \cdot \log (1 - \hat{o}_{x,i}), \quad (4)$$

where $\hat{o}_{x,i}$ is the estimated overlap probability and $o_{x,i}^*$ is the ground truth label. We compute the overlap loss \mathcal{L}_o^Y for the target point cloud similarly.

Feature Loss. Following [64], to ensure that the enhanced features of both point clouds are in the same feature space, we apply an InfoNCE [39] loss on the enhanced features $\bar{\mathbf{F}}_{\mathbf{X}'}$ and $\bar{\mathbf{F}}_{\mathbf{Y}'}$. Given a set of superpoints correspondences $\{(\hat{\mathbf{x}}_i, \hat{\mathbf{y}}_i)\}_{i=1}^K$ and their associated feature representations $\{(\bar{\mathbf{f}}_{\hat{\mathbf{x}}_i}, \bar{\mathbf{f}}_{\hat{\mathbf{y}}_i})\}$, the feature loss is defined as

$$\mathcal{L}_f = -\frac{1}{K} \log \frac{\bar{\mathbf{f}}_{\hat{\mathbf{x}}_i}^T \mathbf{W} \bar{\mathbf{f}}_{\hat{\mathbf{y}}_i}}{\bar{\mathbf{f}}_{\hat{\mathbf{x}}_i}^T \mathbf{W} \bar{\mathbf{f}}_{\hat{\mathbf{y}}_i} + \sum_{j \neq i} \bar{\mathbf{f}}_{\hat{\mathbf{x}}_i}^T \mathbf{W} \bar{\mathbf{f}}_{\hat{\mathbf{y}}_j}}. \quad (5)$$

The linear transformation \mathbf{W} is enforced to be symmetrical by parameterizing it as the sum of an upper triangular matrix \mathbf{U} and its transpose, *i.e.* $\mathbf{W} = \mathbf{U} + \mathbf{U}^T$.

The final loss is a weighted sum of all the losses above with

$$\mathcal{L} = \mathcal{L}_T + \alpha \mathcal{L}_f + \beta (\mathcal{L}_o^X + \mathcal{L}_o^Y), \quad (6)$$

where we set the loss weights $\alpha = 0.1$ and $\beta = 1$ empirically.

Table 1: Registration results on the ModelNet and ModelLoNet benchmarks.

| Methods | ModelNet | | | ModelLoNet | | |
|----------------|--------------|--------------|----------------|--------------|--------------|---------------|
| | RRE↓ | RTE↓ | CD↓ | RRE↓ | RTE↓ | CD↓ |
| PointNetLK | 29.725 | 0.297 | 0.0235 | 48.567 | 0.507 | 0.0367 |
| OMNet | 2.947 | 0.032 | 0.0015 | 6.517 | 0.129 | 0.0074 |
| DCP-v2 | 11.975 | 0.171 | 0.0117 | 16.501 | 0.300 | 0.0268 |
| RPM-Net | 1.712 | 0.018 | 0.00085 | 7.342 | 0.124 | 0.0050 |
| Predator | 1.739 | 0.019 | 0.00089 | 5.235 | 0.132 | 0.0083 |
| RegTR | 1.473 | 0.014 | <u>0.00078</u> | 3.930 | 0.087 | 0.0037 |
| Geotransformer | 1.568 | 0.018 | - | 3.809 | 0.102 | - |
| Ours | 1.247 | 0.011 | 0.00074 | 3.809 | <u>0.088</u> | <u>0.0040</u> |

4 Experiments

We evaluate our approach on two benchmarks with overlap ranging from 10% to 75%. The first dataset we evaluate is on ModelNet with two benchmarks settings following [24, 64] and the second dataset is 3DMatch [68] on two benchmarks following [24, 64, 44, 66].

4.1 Implementation details

Our approach is implemented using the PyTorch framework [41] on a system with an Intel i9-1300K CPU and a single RTX 3090 GPU. The network training is performed with the AdamW optimizer [36], utilizing a learning rate of 0.0001 and a weight decay of 0.0001. For the ModelNet dataset, the network is trained for 400 epochs with a batch size of 4. On the 3DMatch dataset, the network is trained for 50 epochs with a batch size of 4 as well. Training the network requires approximately 22 hours on ModelNet and around 2 days on 3DMatch.

4.2 ModelNet and ModelLoNet Benchmarks

The ModelNet40 [58] dataset comprises of synthetic CAD models. Following the data setting in [24, 64], the point clouds are randomly sampled from mesh faces of the CAD models, cropped and subsampled. For the ModelNet and ModelLoNet benchmarks, the average overlap is 73.5% and 53.6%, respectively. Our network is trained exclusively on ModelNet, and we evaluate its generalization performance on ModelLoNet. For benchmarking the performance of our model we use the Relative Rotation Error (RRE) and Relative translation Error (RTE) as the primary metrics. Following [64], we also calculate the Chamfer Distance (CD) between the registered scan pairs.

The results are shown in Table 1. We compare against correspondence-based approaches [24, 64], coarse-to-fine registration approaches [44], and end-to-end methods [2, 63, 59]. We see that our approach performs well on both benchmarks. Moreover, the low chamfer error suggests that predicted correspondences have very high accuracy. Our approach is also able to outperform methods using post-processing steps like RANSAC [24] by a significant margin, which further strengthens the point that direct superpoints matchings can actually work well for point cloud registration.

4.3 3DMatch and 3DLoMatch Benchmarks

3DMatch [68] is a collection of 62 scenes, from which we use 46 for training, 8 for testing, and 8 for validation following [64, 24, 44]. We use the preprocessed data from [24] which contains point clouds downsampled using a voxel-grid subsampling method. The 3DMatch benchmark contains point clouds pairs with >30% overlap while the 3DLoMatch benchmark contains scan pairs with only 10%-30% overlap. Following [64], we perform training data augmentation by applying small rigid perturbations, jittering, and shuffling of points. Following the literature [24, 44, 68], We report the results of 3DMatch dataset on 5 metrics including RRE, RTE, Registration Recall (RR), Feature Matching Recall (FMR), and Inlier Ratio (IR).

We compare our approach against several approaches including learned corresponding based algorithms [21, 13, 4, 24] and coarse-to-fine approaches [66, 44]. Since the algorithms which use some

Table 2: Registration results on the 3DMatch and 3DLoMatch benchmarks.

| Methods | 3DMatch | | | | | 3DLoMatch | | | | |
|-----------------------|--------------|--------------|-------------|-------------|-------------|--------------|--------------|-------------|-------------|-------------|
| | RRE↓ | RTE↓ | RR↑ | FMR↑ | IR↑ | RRE↓ | RTE↓ | RR↑ | FMR↑ | IR↑ |
| 3DSN | 2.199 | 0.071 | 78.4 | - | - | 3.528 | 0.103 | 33.0 | - | - |
| FCGF | 1.949 | 0.066 | 85.1 | 97.4 | 56.8 | 3.147 | 0.100 | 40.1 | 76.6 | 21.4 |
| D3Feat | 2.161 | 0.067 | 81.6 | 95.6 | 39.0 | 3.361 | 0.103 | 37.2 | 67.3 | 13.2 |
| Predator | 2.029 | 0.064 | 89.0 | 96.6 | 58.8 | 3.048 | 0.093 | 59.8 | 78.6 | 26.7 |
| OMNet | 4.166 | 0.105 | 35.9 | - | - | 7.299 | 0.151 | 8.4 | - | - |
| DGR | 2.103 | 0.067 | 85.3 | - | - | 3.954 | 0.113 | 48.7 | - | - |
| PCAM | 1.808 | 0.059 | 85.5 | - | - | 3.529 | 0.099 | 54.9 | - | - |
| RegTR | 1.567 | 0.049 | 92.0 | - | - | 2.827 | <u>0.077</u> | 64.8 | - | - |
| YOHO | - | - | 90.8 | 98.2 | 64.4 | - | - | 65.2 | 79.4 | 25.9 |
| CofiNet | - | - | 89.3 | <u>98.1</u> | 49.8 | - | - | <u>67.5</u> | <u>83.1</u> | 24.4 |
| Geo-Transformer (SVD) | - | - | 86.5 | - | - | - | - | 59.9 | - | - |
| GeoTransformer (LGR) | 1.625 | 0.053 | 91.5 | 97.7 | <u>70.3</u> | 2.547 | 0.074 | 74.0 | 88.1 | 43.3 |
| Ours | 1.436 | 0.045 | 93.7 | 96.5 | 89.8 | <u>2.553</u> | 0.074 | 65.0 | 76.5 | 57.5 |

post-preprocessing steps like RANSAC perform well only with a large number of interest points, we only show results for the maximum number of sampled points (5000). We also compare against several approaches designed to avoid RANSAC [10, 59, 12].

The quantitative results are shown in Table 2. For the 3DMatch benchmark, our approach outperforms all the previous methods. This implies that in cases of significant overlap (>30%), the superpoint correspondences are very distinctive and accurate. One of the problems associated with superpoint matching in point clouds is the resolution issue, where the correspondences might not actually coincide with each other when transformed with the ground truth transformation matrix due to the subsampling of the point cloud. In our case, the resolution issue is automatically handled by the correlation weights. We also show systematic comparisons with other approaches in Table 3. We can see our model runs fast and is compact.

For the 3DLoMatch benchmark, in comparison to all the approaches that do not use any post-processing, our method performs significantly better than the other approaches. Note that [44] uses LGR as the refinement step to get the best results, but when using all the predicted correspondences with their scores and applying weighted SVD, they get much worse results. This implies that the final set of all the correspondences is not optimal and contains outliers.

In our case, these outliers are filtered by the overlap and correlation values, thus providing accurate correspondences. The validity of the correspondences predicted by our approach can be verified by comparing the mean Inlier Ratio in Table 2. We get the highest mean IR, almost **19%** better than the second-best approach on 3DMatch and **14%** higher in 3DLoMatch.

Table 3: Comparisons of inference speed and number of parameters on the 3DMatch dataset.

| Methods | Matching | e2e | Time | Param |
|----------------|----------------|-----|--------|-------|
| CoFiNet | coarse-to-fine | ✗ | 1.922s | 5.5M |
| GeoTransformer | coarse-to-fine | ✗ | 0.088s | 9.8M |
| RegTR | ✗ | ✓ | 0.063s | 11.8M |
| Ours | direct | ✓ | 0.073s | 7.8M |

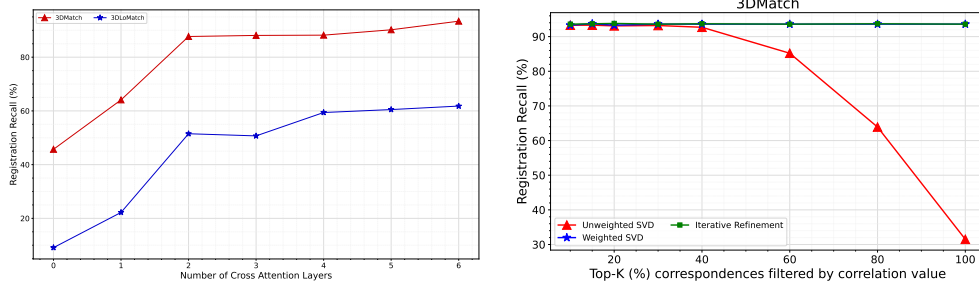
4.4 Ablation Studies

Effectiveness of the feature enhancement. The feature enhancement module is essential in our approach. To assess its effectiveness, we trained various networks with attention layers ranging from 0 to 6. Figure 3 illustrates the performance changes as we increase the number of attention layers. When no feature enhancement is used, the model’s performance is significantly poorer, which is understandable since the source point cloud’s superpoint features lack information about the target point cloud. Performance stabilizes at around 6 attention layers. It is worth noting that increasing the number of layers also leads to higher computation burden.

Using correlation scores for filtering out outliers. To filter out outliers in the predicted correspondences we primarily use the correlation values along with overlap values as weights for weighted

Table 4: Comparisons of different outlier filtering methods.

| Outlier Filtering Method | 3DMatch | | | 3DLoMatch | | | Time |
|------------------------------|--------------|--------------|-------------|--------------|--------------|-------------|--------------|
| | RRE | RTE | RR | RRE | RTE | RR | |
| No filtering | 1.462 | 0.046 | 93.3 | 2.652 | 0.074 | 64.6 | 0.073 |
| Ours + RANSAC-50k | 2.788 | 0.090 | 82.3 | 4.653 | 0.115 | 32.0 | 0.141 |
| Ours (top 15%) + RANSAC-50k | 1.701 | 0.051 | 93.0 | 2.696 | 0.078 | 64.5 | 0.153 |
| Iterative refinement | 1.404 | 0.043 | 93.8 | <u>2.592</u> | 0.071 | 65.7 | <u>0.078</u> |
| Correlation scores (top 15%) | <u>1.436</u> | <u>0.045</u> | <u>93.7</u> | 2.553 | <u>0.074</u> | <u>65.0</u> | 0.073 |

Figure 3: **Left:** Effect of increasing the number of attention layers. **Right:** Comparisons of outlier filtering strategies.

SVD. Since these weights are much lower for outlier values, the registration results are very accurate. If we use unweighted SVD (with equal weights for all the correspondences), the performance drops rapidly with the increase in number of correspondences, as shown in Fig. 1.

We experiment with a simple iterative refinement scheme proposed in [44], where we can iteratively re-estimate the transformation by pruning out outliers. We found that the performance of this refinement saturated after 5 iterations. See Table 4 row 4 for results. Fig. 1 also shows that this approach is quite stable in pruning outliers on different number of correspondences and improves the results by a slight margin.

We also experiment with RANSAC on the set of superpoints correspondences, See Table 4 row 2, 3. But as expected, RANSAC gives slightly worse results while taking more computation time. This implies that using our approach is much more effective in pruning outliers thus eliminating the need for refinement.

Effectiveness of the loss terms. Lastly, we analyze the effectiveness of each loss function. Table 5 shows the results with different loss function configurations. We see that by just using Feature Loss with Transformation loss, the model is able to achieve good performance and using Overlap loss is the final step that helps the model prune remaining outliers. Row 3 in Table 5 again implies that superpoint correspondences are very distinctive.

Table 5: Effectiveness of different loss terms.

| Overlap Feature | | 3DMatch | | | 3DLoMatch | | |
|-----------------|------|--------------|--------------|-------------|--------------|--------------|-------------|
| Loss | Loss | RRE | RTE | RR | RRE | RTE | RR |
| ✗ | ✗ | 2.521 | 0.076 | 76.5 | 5.272 | 0.132 | 31.2 |
| ✓ | ✗ | 2.123 | 0.062 | 79.6 | 4.020 | 0.105 | 37.2 |
| ✗ | ✓ | 1.651 | 0.049 | 90.3 | 2.876 | 0.082 | 58.0 |
| ✓ | ✓ | 1.436 | 0.045 | 93.7 | 2.553 | 0.074 | 65.0 |

5 Limitations and Broader Impacts

We have identified two limitations in the current architecture. First, our approach requires a decent amount of superpoints in the low overlapping region to perform well. Second, our approach samples about 200 best correspondences, but for the low overlapping region only a few of them lie on the overlapping region thus making it hard for the network to achieve good performance on 3DLoMatch benchmark. Instead of regularly downsampling, structure-aware sampling strategies are needed.

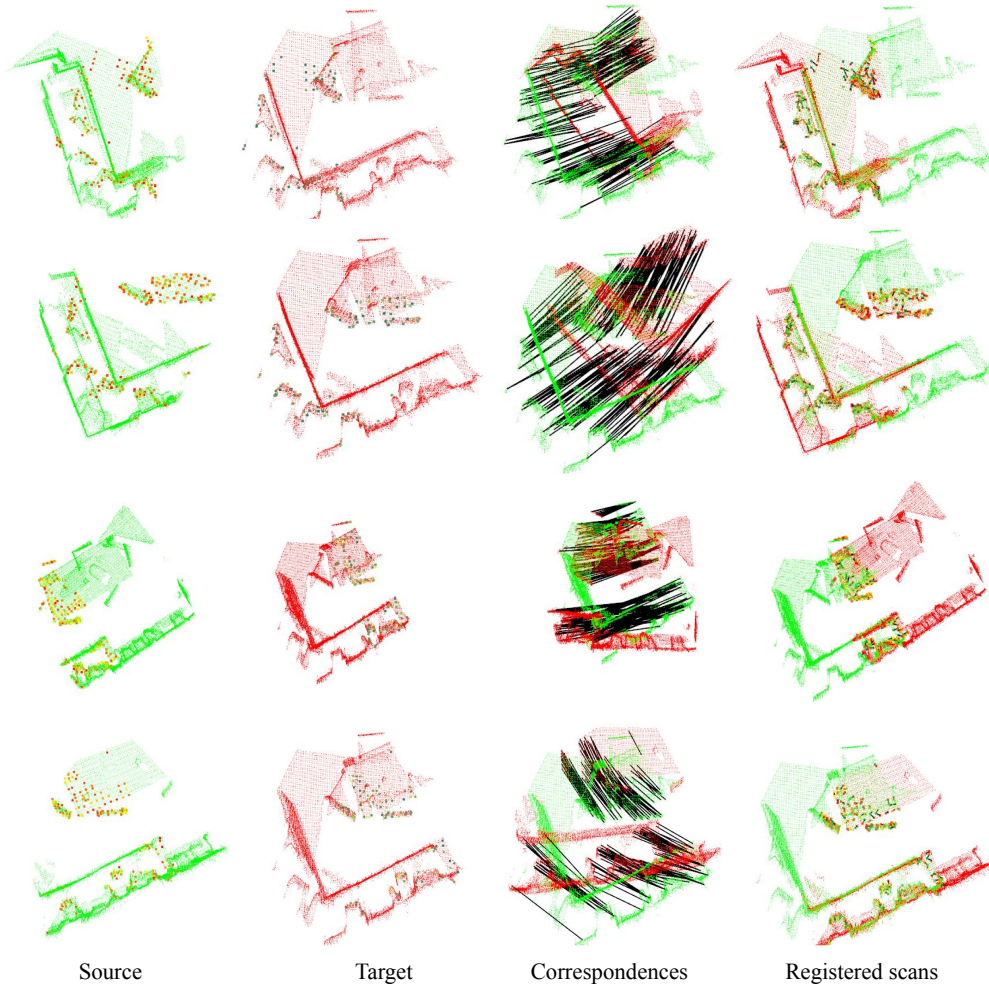


Figure 4: Qualitative Results on 3Dmatch dataset: The source cloud is shown in Green with the red color representing the matched superpoints. Similarly target cloud is in red color with matching superpoints in green color.

This research has the potential to significantly impact the fields of 3D computer vision and robotics, as well as any domains that rely on accurate and efficient point cloud registration, such as autonomous navigation, 3D mapping, and augmented reality. By introducing a simple yet effective approach for directly matching superpoints in an end-to-end manner, the research not only speeds up the registration process but also enhances its robustness by effectively filtering out outliers without any postprocessing refinement.

6 Conclusion

We introduce a straightforward yet highly effective method for point cloud registration that offers simplicity in understanding and implementation. Our approach directly matches superpoints to establish correspondences, enabling the computation of rigid transformations and correlation weights. To enhance performance in low overlap regions, we augment the correlation weights with predicted overlap values. Experimental evaluations on the 3DMatch and ModelNet datasets demonstrate the efficacy of our approach across different overlap scenarios. Notably, our approach is computationally efficient, robust to outliers, and does not require post-processing steps, making it suitable for real-time

applications. In the future, we plan to extend its application to cross-modalities such as image-to-image and image-to-point cloud registration.

References

- [1] Sheng Ao, Qingyong Hu, Bo Yang, Andrew Markham, and Yulan Guo. Spinnet: Learning a general surface descriptor for 3d point cloud registration. In *CVPR*, 2021.
- [2] Yasuhiro Aoki, Hunter Goforth, Rangaprasad Arun Srivatsan, and Simon Lucey. Pointnetlk: Robust & efficient point cloud registration using pointnet. In *CVPR*, 2019.
- [3] Xuyang Bai, Zixin Luo, Lei Zhou, Hongkai Chen, Lei Li, Zeyu Hu, Hongbo Fu, and Chiew-Lan Tai. Pointdsc: Robust point cloud registration using deep spatial consistency. In *CVPR*, 2021.
- [4] Xuyang Bai, Zixin Luo, Lei Zhou, Hongbo Fu, Long Quan, and Chiew-Lan Tai. D3feat: Joint learning of dense detection and description of 3d local features. In *CVPR*, 2020.
- [5] Paul J Besl and Neil D McKay. Method for registration of 3-d shapes. In *Sensor fusion IV: control paradigms and data structures*, 1992.
- [6] Sofien Bouaziz, Andrea Tagliasacchi, and Mark Pauly. Sparse iterative closest point. In *Computer graphics forum*, 2013.
- [7] Eric Brachmann, Alexander Krull, Sebastian Nowozin, Jamie Shotton, Frank Michel, Stefan Gumhold, and Carsten Rother. Dsac-differentiable ransac for camera localization. In *CVPR*, 2017.
- [8] Dylan Campbell and Lars Petersson. Gogma: Globally-optimal gaussian mixture alignment. In *CVPR*, 2016.
- [9] Dylan Campbell, Lars Petersson, Laurent Kneip, Hongdong Li, and Stephen Gould. The alignment of the spheres: Globally-optimal spherical mixture alignment for camera pose estimation. In *CVPR*, 2019.
- [10] Anh-Quan Cao, Gilles Puy, Alexandre Boulch, and Renaud Marlet. Pcam: Product of cross-attention matrices for rigid registration of point clouds. In *ICCV*, 2021.
- [11] Dmitry Chetverikov, Dmitry Svirko, Dmitry Stepanov, and Pavel Krsek. The trimmed iterative closest point algorithm. In *ICPR*, 2002.
- [12] Christopher Choy, Wei Dong, and Vladlen Koltun. Deep global registration. In *CVPR*, 2020.
- [13] Christopher Choy, Jaesik Park, and Vladlen Koltun. Fully convolutional geometric features. In *CVPR*, 2019.
- [14] Haowen Deng, Tolga Birdal, and Slobodan Ilic. Ppf-foldnet: Unsupervised learning of rotation invariant 3d local descriptors. In *ECCV*, 2018.
- [15] Haowen Deng, Tolga Birdal, and Slobodan Ilic. Ppfnet: Global context aware local features for robust 3d point matching. In *CVPR*, 2018.
- [16] Jean-Emmanuel Deschaud. IMLS-SLAM: scan-to-model matching based on 3d data. In *ICRA*, 2018.
- [17] Benjamin Eckart, Kihwan Kim, and Jan Kautz. Hgmr: Hierarchical gaussian mixtures for adaptive 3d registration. In *ECCV*, 2018.
- [18] Martin A Fischler and Robert C Bolles. Random sample consensus: a paradigm for model fitting with applications to image analysis and automated cartography. *Communications of the ACM*, 1981.
- [19] Kexue Fu, Shaolei Liu, Xiaoyuan Luo, and Manning Wang. Robust point cloud registration framework based on deep graph matching. In *CVPR*, 2021.
- [20] Zan Gojcic, Caifa Zhou, Jan D Wegner, Leonidas J Guibas, and Tolga Birdal. Learning multiview 3d point cloud registration. In *CVPR*, 2020.
- [21] Zan Gojcic, Caifa Zhou, Jan D Wegner, and Andreas Wieser. The perfect match: 3d point cloud matching with smoothed densities. In *CVPR*, 2019.
- [22] Johannes Groß, Aljoša Ošep, and Bastian Leibe. Alignnet-3d: Fast point cloud registration of partially observed objects. In *3DV*, 2019.
- [23] Kaiming He, Xiangyu Zhang, Shaoqing Ren, and Jian Sun. Deep residual learning for image recognition. In *CVPR*, 2016.
- [24] Shengyu Huang, Zan Gojcic, Mikhail Usvyatsov, Andreas Wieser, and Konrad Schindler. Predator: Registration of 3d point clouds with low overlap. In *CVPR*, 2021.
- [25] Xiaoshui Huang, Guofeng Mei, and Jian Zhang. Feature-metric registration: A fast semi-supervised approach for robust point cloud registration without correspondences. In *CVPR*, 2020.

- [26] Shahram Izadi, Richard A. Newcombe, David Kim, Otmar Hilliges, David Molyneaux, Steve Hodges, Pushmeet Kohli, Jamie Shotton, Andrew J. Davison, and Andrew W. Fitzgibbon. Kinectfusion: real-time dynamic 3d surface reconstruction and interaction. In *SIGGRAPH*, 2011.
- [27] Bing Jian and Baba C Vemuri. Robust point set registration using gaussian mixture models. *TPAMI*, 2010.
- [28] Wolfgang Kabsch. A solution for the best rotation to relate two sets of vectors. *Acta Crystallographica Section A: Crystal Physics, Diffraction, Theoretical and General Crystallography*, 1976.
- [29] Marc Khoury, Qian-Yi Zhou, and Vladlen Koltun. Learning compact geometric features. In *ICCV*, 2017.
- [30] Junha Lee, Seungwook Kim, Minsu Cho, and Jaesik Park. Deep hough voting for robust global registration. In *ICCV*, 2021.
- [31] Jiahao Li, Changhao Zhang, Ziyao Xu, Hangning Zhou, and Chi Zhang. Iterative distance-aware similarity matrix convolution with mutual-supervised point elimination for efficient point cloud registration. In *ECCV*, 2020.
- [32] Jiaxin Li and Gim Hee Lee. Usip: Unsupervised stable interest point detection from 3d point clouds. *ICCV*, 2019.
- [33] Xueqian Li, Jhony Kaesemodel Pontes, and Simon Lucey. Pointnetlk revisited. In *CVPR*, 2021.
- [34] Ying Li, Lingfei Ma, Zilong Zhong, Fei Liu, Michael A. Chapman, Dongpu Cao, and Jonathan Li. Deep learning for lidar point clouds in autonomous driving: A review. *IEEE Transactions on Neural Networks and Learning Systems*, 2021.
- [35] Yinlong Liu, Chen Wang, Zhijian Song, and Manning Wang. Efficient global point cloud registration by matching rotation invariant features through translation search. In *ECCV*, 2018.
- [36] Ilya Loshchilov and Frank Hutter. Decoupled weight decay regularization. In *ICLR*, 2019.
- [37] Weixin Lu, Yao Zhou, Guowei Wan, Shenhua Hou, and Shiyu Song. L3-net: Towards learning based lidar localization for autonomous driving. In *CVPR*, 2019.
- [38] Guofeng Mei, Xiaoshui Huang, Jian Zhang, and Qiang Wu. Overlap-guided coarse-to-fine correspondence prediction for point cloud registration. In *ICME*, 2022.
- [39] Aaron van den Oord, Yazhe Li, and Oriol Vinyals. Representation learning with contrastive predictive coding. *arXiv*, 2018.
- [40] G Dias Pais, Srikumar Ramalingam, Venu Madhav Govindu, Jacinto C Nascimento, Rama Chellappa, and Pedro Miraldo. 3dregnet: A deep neural network for 3d point registration. In *CVPR*, 2020.
- [41] Adam Paszke, Sam Gross, Francisco Massa, Adam Lerer, James Bradbury, Gregory Chanan, Trevor Killeen, Zeming Lin, Natalia Gimeshein, Luca Antiga, et al. Pytorch: An imperative style, high-performance deep learning library. *NeurIPS*, 2019.
- [42] Charles Ruizhongtai Qi, Hao Su, Kaichun Mo, and Leonidas J. Guibas. Pointnet: Deep learning on point sets for 3d classification and segmentation. In *CVPR*, 2017.
- [43] Charles Ruizhongtai Qi, Li Yi, Hao Su, and Leonidas J. Guibas. Pointnet++: Deep hierarchical feature learning on point sets in a metric space. In *NeurIPS*, 2017.
- [44] Zheng Qin, Hao Yu, Changjian Wang, Yulan Guo, Yuxing Peng, and Kai Xu. Geometric transformer for fast and robust point cloud registration. In *CVPR*, 2022.
- [45] Szymon Rusinkiewicz. A symmetric objective function for icp. *ACM Transactions on Graphics (TOG)*, 2019.
- [46] Szymon Rusinkiewicz and Marc Levoy. Efficient variants of the icp algorithm. In *Proceedings third international conference on 3-D digital imaging and modeling*, 2001.
- [47] Radu Bogdan Rusu, Nico Blodow, and Michael Beetz. Fast point feature histograms (fpfh) for 3d registration. In *ICRA*, 2009.
- [48] Vinit Sarode, Xueqian Li, Hunter Goforth, Yasuhiro Aoki, Rangaprasad Arun Srivatsan, Simon Lucey, and Howie Choset. Pcrnet: Point cloud registration network using pointnet encoding. *arXiv*, 2019.
- [49] Aleksandr Segal, Dirk Haehnel, and Sebastian Thrun. Generalized-icp. In *Robotics: science and systems*, 2009.
- [50] Tixiao Shan and Brendan Englot. Lego-loam: Lightweight and ground-optimized lidar odometry and mapping on variable terrain. In *IROS*, 2018.
- [51] Hugues Thomas, Charles R Qi, Jean-Emmanuel Deschaud, Beatriz Marcotegui, François Goulette, and Leonidas J Guibas. Kpconv: Flexible and deformable convolution for point clouds. In *ICCV*, 2019.
- [52] Federico Tombari, Samuele Salti, and Luigi Di Stefano. Unique signatures of histograms for local surface description. In *ECCV*, 2010.

- [53] S. Umeyama. Least-squares estimation of transformation parameters between two point patterns. *TPAMI*, 1991.
- [54] Ashish Vaswani, Noam Shazeer, Niki Parmar, Jakob Uszkoreit, Llion Jones, Aidan N Gomez, Łukasz Kaiser, and Illia Polosukhin. Attention is all you need. In *NeurIPS*, 2017.
- [55] Haiping Wang, Yuan Liu, Zhen Dong, and Wenping Wang. You only hypothesize once: Point cloud registration with rotation-equivariant descriptors. In *ACM MM*, 2022.
- [56] Yue Wang and Justin Solomon. Prnet: self-supervised learning for partial-to-partial registration. In *NeurIPS*, 2019.
- [57] Yue Wang and Justin M Solomon. Deep closest point: Learning representations for point cloud registration. In *ICCV*, 2019.
- [58] Zhirong Wu, Shuran Song, Aditya Khosla, Fisher Yu, Linguang Zhang, Xiaoou Tang, and Jianxiong Xiao. 3d shapenets: A deep representation for volumetric shapes. In *CVPR*, 2015.
- [59] Hao Xu, Shuaicheng Liu, Guangfu Wang, Guanghui Liu, and Bing Zeng. Omnet: Learning overlapping mask for partial-to-partial point cloud registration. In *ICCV*, 2021.
- [60] Haofei Xu, Jing Zhang, Jianfei Cai, Hamid Rezatofighi, and Dacheng Tao. Gmflow: Learning optical flow via global matching. In *CVPR*, 2022.
- [61] Jiaolong Yang, Hongdong Li, Dylan Campbell, and Yunde Jia. Go-icp: A globally optimal solution to 3d icp point-set registration. *TPAMI*, 2015.
- [62] Zi Jian Yew and Gim Hee Lee. 3dfeat-net: Weakly supervised local 3d features for point cloud registration. In *ECCV*, 2018.
- [63] Zi Jian Yew and Gim Hee Lee. Rpm-net: Robust point matching using learned features. In *CVPR*, 2020.
- [64] Zi Jian Yew and Gim hee Lee. Regtr: End-to-end point cloud correspondences with transformers. In *CVPR*, 2022.
- [65] Kwang Moo Yi, Eduard Trulls, Yuki Ono, Vincent Lepetit, Mathieu Salzmann, and Pascal Fua. Learning to find good correspondences. In *CVPR*, 2018.
- [66] Hao Yu, Fu Li, Mahdi Saleh, Benjamin Busam, and Slobodan Ilic. Cofinet: Reliable coarse-to-fine correspondences for robust pointcloud registration. *NeurIPS*, 2021.
- [67] Wentao Yuan, Benjamin Eckart, Kihwan Kim, Varun Jampani, Dieter Fox, and Jan Kautz. Deepgmr: Learning latent gaussian mixture models for registration. In *ECCV*, 2020.
- [68] Andy Zeng, Shuran Song, Matthias Nießner, Matthew Fisher, Jianxiong Xiao, and Thomas Funkhouser. 3dmatch: Learning local geometric descriptors from rgb-d reconstructions. In *CVPR*, 2017.

A Appendix

A.1 Network Architecture

The network architecture for the KPConv backbone used is shown in Fig. 5 and the architecture for the Feature Enhancement module is shown in Fig. 6.

We do not downsample the point cloud by a large factor in the backbone unlike other methods [44, 64] as this leads to a very low resolution in the overlapping region of the point cloud pair. Since, we are training the network to learn correlations between the downsampled superpoints, it is beneficial to have a moderately larger number of points.

A.2 Evaluation Metrics

We report Registration Recall (RR), Relative Rotation Error (RRE), Relative Translation Error (RTE), Feature Matching Recall (FMR), and Inlier Ratio (IR) for the 3DMatch dataset following common practice [44, 64, 24, 66, 4]. For ModelNet dataset, we report RRE, RTE, and Chamfer Distance Error (CD) following [64, 24, 59].

A.2.1 3DMatch/3DLoMatch

Inlier Ratio is the fraction of inlier correspondences in all predicted correspondences. Corresponding points are considered inliers if the distance between them under the ground-truth transformation is smaller than $\tau_1 = 10cm$.

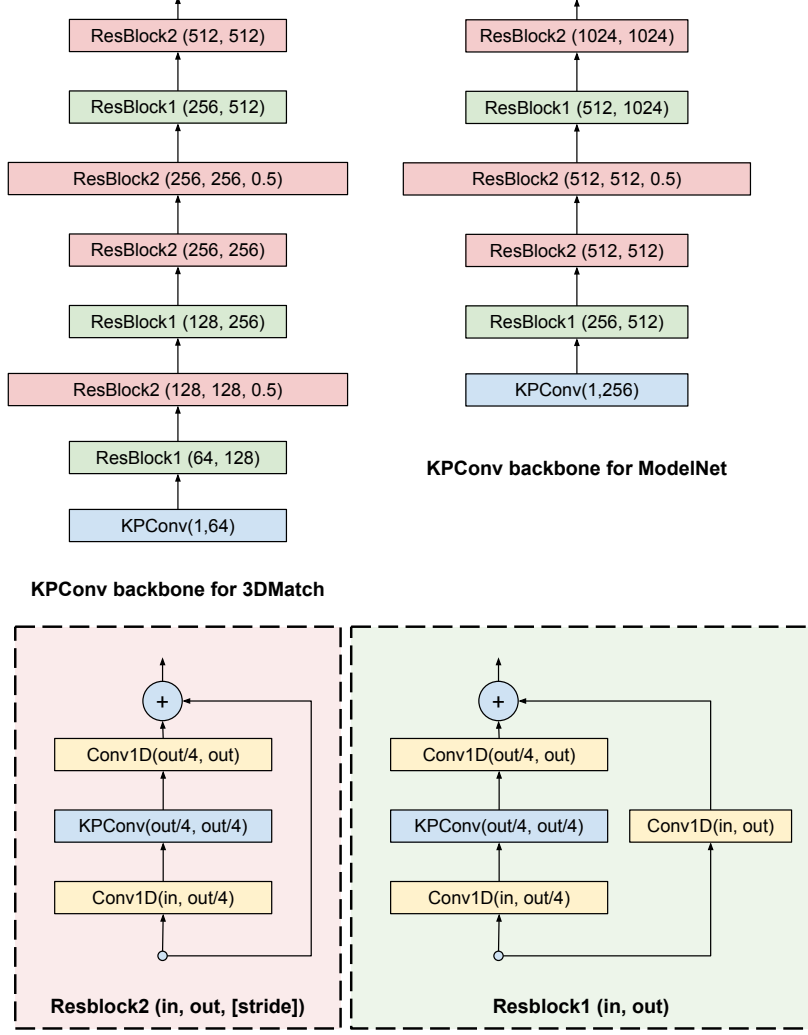


Figure 5: Network Architecture of the KPConv backbone for 3DMatch and ModelNet dataset. We do not downsample the point cloud by a large factor to maintain resolution on the overlapping region of the point cloud pair.

$$\text{IR}(\mathbf{X}, \mathbf{Y}) = \frac{1}{|\hat{\mathcal{C}}|} \sum_{(\mathbf{x}_i, \mathbf{y}_i) \in \hat{\mathcal{C}}} \mathbb{I}[\|\bar{\mathbf{T}}_{\mathbf{Y}}^{\mathbf{X}}(\mathbf{x}_i) - \mathbf{y}_i\|_2 < \tau_1], \quad (7)$$

where $\mathbb{I}[\cdot]$ is the Iversion bracket, $\bar{\mathbf{T}}_{\mathbf{Y}}^{\mathbf{X}}$ is the ground-truth transformation and $(\mathbf{x}_i, \mathbf{y}_i) \in \hat{\mathcal{C}}$ are the predicted correspondences.

Feature Matching Recall is the fraction of point cloud pairs whose inlier ratio is above $\tau_2 = 0.05$. It indicates the likelihood of recovering the optimal transformation between two point clouds. It is a good indicator for methods which use post-processing refinement steps like RANSAC [66, 44, 24] as having a higher FMR increases the probability of recovering the correct transformation. If the total number of point cloud pairs in the test set is \mathcal{N} , FMR can be calculated as

$$\text{FMR} = \frac{1}{\mathcal{N}} \sum_{i=1}^{\mathcal{N}} \mathbb{I}[\text{IR} > \tau_2]. \quad (8)$$

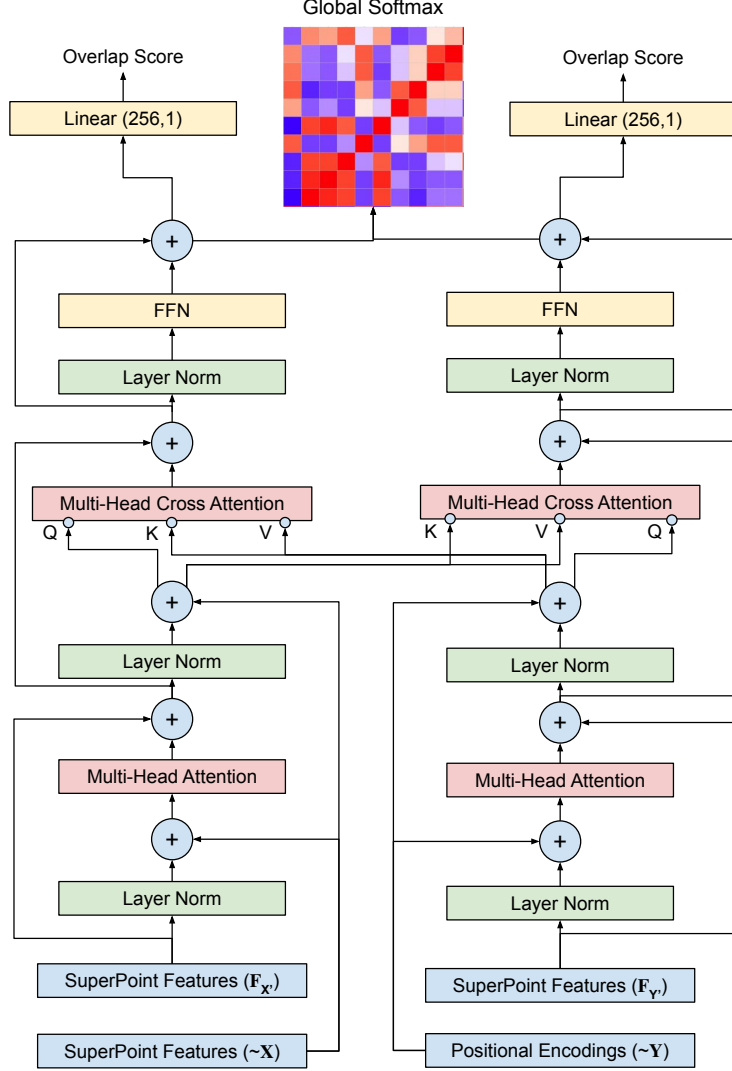


Figure 6: Network architecture of the Feature Enhancement Module. The architecture is shown for just one block of self-attention and cross-attention layers but can be extended similarly for improvement in performance.

Registration Recall represents the fraction of point cloud pairs whose Root Mean Square Error (RMSE) is less than $\tau_3 = 20cm$. RR directly measures the effectiveness of the registration algorithm.

$$RR = \frac{1}{\mathcal{N}} \sum_{i=1}^{\mathcal{N}} \left\| \sqrt{\frac{1}{|\mathcal{C}^*|} \sum_{(\mathbf{x}_i, \mathbf{y}_i) \in \mathcal{C}^*} \|\mathbf{T}_{\mathbf{Y}}^{\mathbf{X}}(\mathbf{x}_i) - \mathbf{y}_i\|_2^2} < \tau_3 \right\|, \quad (9)$$

where \mathcal{C}^* is the set of ground truth correspondences and $\mathbf{T}_{\mathbf{Y}}^{\mathbf{X}}$ is the predicted transformation matrix.

Relative Rotation Error and **Relative Translation Error** are the rotation and translation errors between the ground truth transformation matrix $\bar{\mathbf{T}}_{\mathbf{Y}}^{\mathbf{X}} \in SE(3)$ and the predicted transformation $\mathbf{T}_{\mathbf{Y}}^{\mathbf{X}} \in SE(3)$. We can obtain $\mathbf{R} \in SO(3)$, $\bar{\mathbf{R}} \in SO(3)$, $\mathbf{t} \in \mathbf{R}^3$ and $\bar{\mathbf{t}} \in \mathbf{R}^3$ as the predicted rotation matrix, ground truth rotation matrix, predicted translation vector and ground truth translation vector respectively. Thus, RRE and RTE can be calculated as follows

Table 6: Scene-wise registration results on the 3DMatch and 3DLoMatch benchmarks.

| Method | 3DMatch | | | | | | | | | | 3DLoMatch | | | | | | | | | |
|---|--------------|--------------|--------------|--------------|--------------|--------------|--------------|--------------|--------------|--|--------------|--------------|--------------|--------------|--------------|--------------|--------------|--------------|--------------|--|
| | Kitchen | Home 1 | Home 2 | Hotel 1 | Hotel 2 | Hotel 3 | Study | Lab | Mean | | Kitchen | Home 1 | Home 2 | Hotel 1 | Hotel 2 | Hotel 3 | Study | Lab | Mean | |
| <i>Registration Recall (%)</i> ↑ | | | | | | | | | | | | | | | | | | | | |
| 3DSN | 90.6 | 90.6 | 65.4 | 89.6 | 82.1 | 80.8 | 68.4 | 60.0 | 78.4 | | 51.4 | 25.9 | 44.1 | 41.1 | 30.7 | 36.6 | 14.0 | 20.3 | 33.0 | |
| FCGF | <u>98.0</u> | 94.3 | 68.6 | 96.7 | 91.0 | 84.6 | 76.1 | 71.1 | 85.1 | | 60.8 | 42.2 | 53.6 | 53.1 | 38.0 | 26.8 | 16.1 | 30.4 | 40.1 | |
| D3Feat | 96.0 | 86.8 | 67.3 | 90.7 | 88.5 | 80.8 | 78.2 | 64.4 | 81.6 | | 49.7 | 37.2 | 47.3 | 47.8 | 36.5 | 31.7 | 15.7 | 31.9 | 37.2 | |
| Predator | 97.6 | <u>97.2</u> | 74.8 | 98.9 | 96.2 | <u>88.5</u> | 85.9 | 73.3 | 89.0 | | 71.5 | 58.2 | 60.8 | 77.5 | 64.2 | 61.0 | 45.8 | 39.1 | 59.8 | |
| CoFiNet | 96.4 | 99.1 | 73.6 | 95.6 | 91.0 | 84.6 | 89.7 | 84.4 | 89.3 | | <u>76.7</u> | <u>66.7</u> | 64.0 | <u>81.3</u> | <u>65.0</u> | 63.4 | <u>53.4</u> | 69.6 | <u>67.5</u> | |
| RegTR | 97.8 | 90.6 | 75.5 | <u>97.8</u> | <u>94.9</u> | 100 | 88.5 | <u>91.1</u> | <u>92.0</u> | | 66.2 | 58.5 | 64.9 | 72.7 | 61.3 | 70.7 | 53.0 | 71.0 | 64.8 | |
| GeoT | 98.9 | <u>97.2</u> | <u>81.1</u> | 98.9 | 89.7 | <u>88.5</u> | 88.9 | 88.9 | 91.5 | | 85.9 | 73.5 | 72.5 | 89.5 | 73.2 | <u>66.7</u> | 55.3 | <u>75.7</u> | 74.0 | |
| Ours | 97.6 | 88.7 | 87.4 | <u>97.8</u> | 93.6 | 100 | 87.2 | 97.8 | 93.7 | | 62.3 | 55.3 | <u>69.4</u> | 72.2 | 62.0 | 45.6 | 46.2 | 76.8 | 65.0 | |
| <i>Relative Rotation Error (°)</i> ↓ | | | | | | | | | | | | | | | | | | | | |
| 3DSN | 1.926 | 1.843 | 2.324 | 2.041 | 1.952 | 2.908 | 2.296 | 2.301 | 2.199 | | 3.020 | 3.898 | 3.427 | 3.196 | 3.217 | 3.328 | 4.325 | 3.814 | 3.528 | |
| FCGF | 1.767 | 1.849 | 2.210 | 1.867 | 1.667 | 2.417 | 2.024 | 1.792 | 1.949 | | 2.904 | 3.229 | 3.277 | 2.768 | 2.801 | 2.822 | 3.372 | 4.006 | 3.147 | |
| D3Feat | 2.016 | 2.029 | 2.425 | 1.990 | 1.967 | 2.400 | 2.346 | 2.115 | 2.161 | | 3.226 | 3.492 | 3.373 | 3.330 | 3.165 | 2.972 | 3.708 | 3.619 | 3.361 | |
| Predator | 1.861 | 1.806 | 2.473 | 2.045 | 1.600 | 2.458 | 2.067 | 1.926 | 2.029 | | 3.079 | 2.637 | 3.220 | 2.694 | 2.907 | 3.390 | 3.046 | 3.412 | 3.048 | |
| CoFiNet | 1.910 | 1.835 | 2.316 | 1.767 | 1.753 | 1.639 | 2.527 | 2.345 | 2.011 | | 3.213 | 3.119 | 3.711 | 2.842 | 2.897 | 3.194 | 4.126 | 3.138 | 3.280 | |
| RegTR | 1.729 | <u>1.34</u> | <u>1.79</u> | 1.639 | <u>1.28</u> | 1.810 | <u>1.57</u> | <u>1.35</u> | <u>1.56</u> | | 3.366 | 2.446 | 3.244 | 2.732 | 2.439 | 2.919 | 3.044 | 2.428 | 2.827 | |
| GeoT | <u>1.79</u> | 1.353 | <u>1.79</u> | <u>1.52</u> | 1.328 | <u>1.57</u> | 1.952 | 1.678 | 1.625 | | <u>2.35</u> | <u>2.30</u> | 2.541 | 2.455 | <u>2.49</u> | 2.504 | 3.01 | 2.716 | 2.547 | |
| Ours | 1.780 | 1.272 | 1.596 | 1.457 | 1.239 | 1.456 | 1.492 | 1.196 | 1.436 | | 2.330 | 2.281 | <u>2.59</u> | <u>2.72</u> | 2.520 | <u>2.58</u> | 2.775 | <u>2.61</u> | <u>2.55</u> | |
| <i>Relative Translation Error (m)</i> ↓ | | | | | | | | | | | | | | | | | | | | |
| 3DSN | 0.059 | 0.070 | 0.079 | 0.065 | 0.074 | 0.062 | 0.093 | 0.065 | 0.071 | | 0.082 | 0.098 | 0.096 | 0.101 | 0.080 | 0.089 | 0.158 | 0.120 | 0.103 | |
| FCGF | 0.053 | 0.056 | 0.071 | 0.062 | 0.061 | 0.055 | 0.082 | 0.090 | 0.066 | | 0.084 | 0.097 | 0.076 | 0.101 | 0.084 | 0.077 | 0.144 | 0.140 | 0.100 | |
| D3Feat | 0.055 | 0.065 | 0.080 | 0.064 | 0.078 | 0.049 | 0.083 | 0.064 | 0.067 | | 0.088 | 0.101 | 0.086 | 0.099 | 0.092 | 0.075 | 0.146 | 0.135 | 0.103 | |
| Predator | 0.048 | 0.055 | 0.070 | 0.073 | 0.060 | 0.065 | 0.080 | 0.063 | 0.064 | | 0.081 | 0.080 | 0.084 | 0.099 | 0.096 | 0.077 | 0.101 | 0.130 | 0.093 | |
| CoFiNet | 0.047 | 0.059 | 0.063 | 0.063 | 0.058 | 0.044 | 0.087 | 0.075 | 0.062 | | 0.080 | 0.078 | 0.078 | 0.099 | 0.086 | 0.077 | 0.131 | 0.123 | 0.094 | |
| RegTR | 0.040 | <u>0.041</u> | 0.057 | 0.057 | 0.042 | <u>0.039</u> | <u>0.054</u> | 0.058 | <u>0.049</u> | | 0.079 | 0.064 | 0.078 | 0.094 | <u>0.074</u> | 0.060 | <u>0.093</u> | 0.077 | <u>0.077</u> | |
| GeoT | <u>0.042</u> | 0.046 | <u>0.059</u> | <u>0.055</u> | 0.046 | 0.050 | 0.073 | 0.053 | <u>0.053</u> | | <u>0.062</u> | 0.070 | <u>0.071</u> | 0.080 | 0.075 | 0.049 | 0.107 | <u>0.083</u> | 0.074 | |
| Ours | 0.043 | 0.037 | 0.061 | 0.051 | <u>0.044</u> | 0.029 | 0.048 | 0.044 | 0.045 | | 0.061 | <u>0.068</u> | 0.068 | <u>0.088</u> | 0.071 | <u>0.054</u> | 0.091 | 0.091 | 0.074 | |

$$\text{RRE} = \arccos\left(\frac{\text{trace}(\mathbf{R}^T \bar{\mathbf{R}}) - 1}{2}\right), \quad \text{RTE} = \|\mathbf{t} - \bar{\mathbf{t}}\|. \quad (10)$$

A.2.2 ModelNet/ModelLoNet

Chamfer Distance measures the dissimilarity or discrepancy between two sets of points or point clouds. It quantifies the minimum average distance between each point in one set and its nearest neighbor in the other set. It provides a measure of how well two point clouds align or match with each other, with lower values indicating a better alignment.

$$\text{CD}(\mathbf{X}, \mathbf{Y}) = \sum_{x \in \mathbf{X}} \min_{y \in \mathbf{Y}} \|y - \mathbf{T}_{\mathbf{Y}}^{\mathbf{X}}(x)\|_2 + \sum_{y \in \mathbf{Y}} \min_{x \in \mathbf{X}} \|y - \mathbf{T}_{\mathbf{X}}^{\mathbf{Y}}(y)\|_2, \quad (11)$$

where \mathbf{X} and \mathbf{Y} represent the sets of points in two point clouds, $\|\cdot\|_2$ denotes the Euclidean distance and $\mathbf{T}_{\mathbf{Y}}^{\mathbf{X}}$ is the predicted transformation between point clouds \mathbf{X} , and \mathbf{Y} .

A.3 Additional Results

Table 6 shows the scene-wise registration results on the 3DMatch and 3DLoMatch benchmarks. Following literature [44, 64, 24], we only calculate mean RRE and RTE for the successfully registered scan pairs. For the 3DMatch benchmark, our method outperforms other methods in every metric. Our methods achieves not only the highest registration recall, but also the lowest mean RRE and RTE. This implies that the for all the successfully registered points clouds, the predicted correspondences and their correlation values are very accurate. For the 3DLoMatch benchmark, our method outperforms every method which does not use post-processing refinement like RegTR, while giving the lowest RRE and RTE values. In comparison to approaches which use post-processing refinement like GeoTransformer, Predator, and CoFiNet, the performance gap is expected as the predictions in 3DLoMatch contain a much higher number of outliers. But the gap is minor and our approach runs faster.

A.4 Iterative Pose Refinement

We experiment with a simple iterative refinement scheme proposed in [44], where we can iteratively re-estimate the transformation by pruning out outliers.

$$\mathbf{R}, \mathbf{t} = \max_{\mathbf{R}_i, \mathbf{t}_i} \sum_i \mathbb{I}[\|\mathbf{R}\mathbf{x}_i + \mathbf{t} - \mathbf{y}_i\|^2 < \tau_a], \quad (12)$$

where $\mathbb{I}[\cdot]$ is the Iverson bracket, τ_a is the threshold radius (10 cm for 3DMatch and 5cm for ModelNet dataset) and $(\mathbf{x}_i, \mathbf{y}_i) \in \hat{\mathcal{C}}$ are the predicted correspondences. We can iteratively re-estimate the transformation with the matches that satisfy the criteria and prune out the outliers in every step. We can use this pose refinement in cases of very low overlap cases like the 3DLoMatch benchmark. Although we do not use this refinement in our results in the paper, we provide the analysis for practical usage. For our tests, we found that the performance of this refinement saturated after 5 iterations, as shown in Fig. 7.

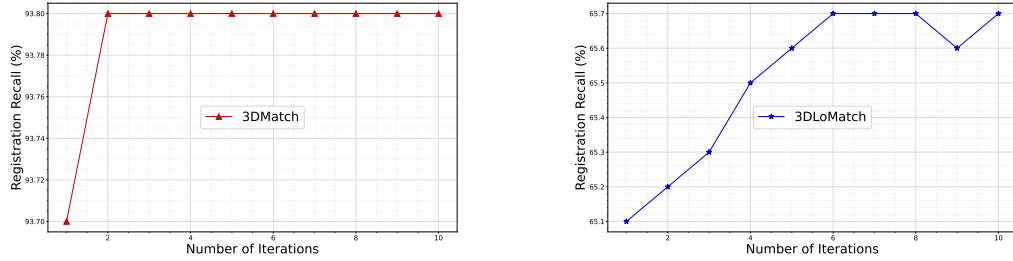


Figure 7: Improvement in Registration Recall on increasing the number of iterations for pose refinement. We see that the performance saturates after the 5th iteration for 3DLoMatch and after 2 iterations for 3DMatch.

A.5 Qualitative Results

We provide more visual results in Fig. 8 and Fig. 9.

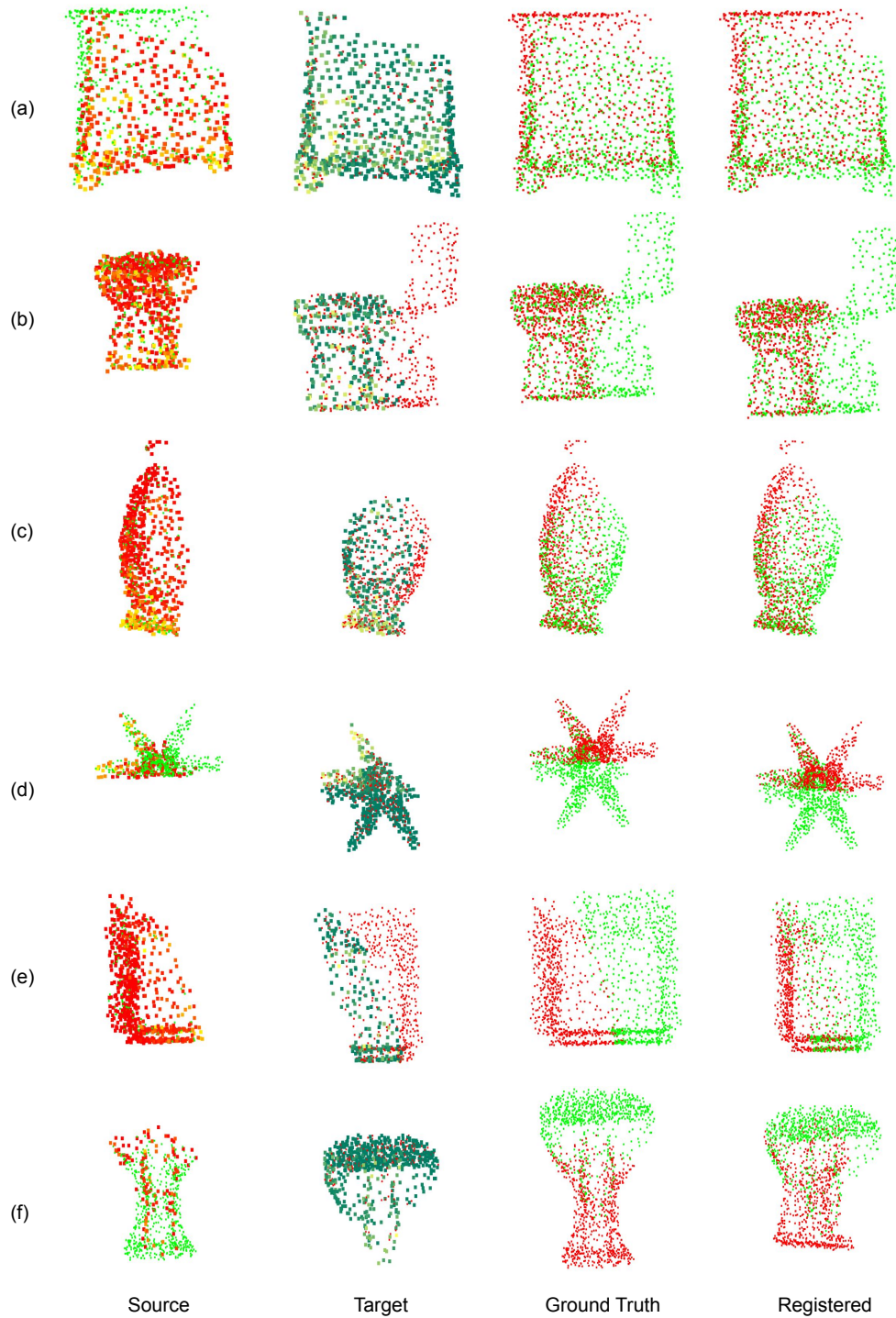


Figure 8: Qualitative Results on the ModelLoNet dataset. Row (a)-(d) show the cases with successful registration. While the rows (e) and (f) show the failure cases. The source cloud is shown in Green with the red color representing for the matched superpoints. Similarly target cloud is in red color with matching superpoints in green color. We see that our approach only fails in cases which are very ambiguous.

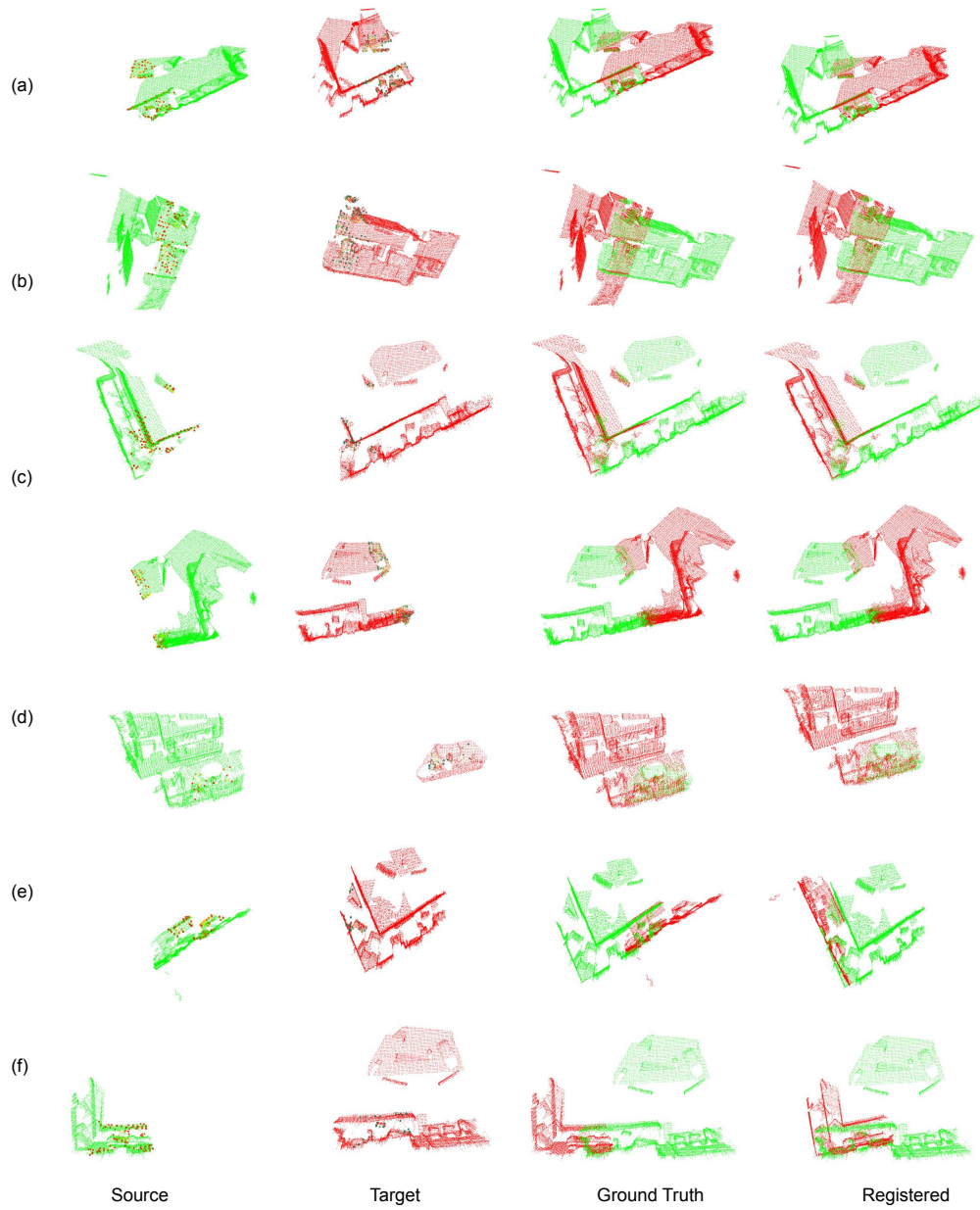


Figure 9: Qualitative Results on the 3DLoMatch dataset. Row (a)-(d) show the cases with successful registration. While the rows (e) and (f) show the failure cases. The source cloud is shown in Green with the red color representing for the matched superpoints. Similarly target cloud is in red color with matching superpoints in green color.